catalysts

MDPI

*Article*

# Fluoride-Doped $TiO_2$ Photocatalyst with Enhanced Activity for Stable Pollutant Degradation

**Aida M. Díez [1,2,*], Iván Núñez [1], Marta Pazos [2], M. Ángeles Sanromán [2] and Yury V. Kolen'ko [1]**

[1] Nanochemistry Research Group, International Iberian Nanotechnology Laboratory, Avenida Mestre José Veiga, 4715-330 Braga, Portugal
[2] CINTECX, Universidade de Vigo, Grupo de Bioingeniería y Procesos Sostenibles, Departamento de Ingeniería Química, Campus Lagoas-Marcosende, 36310 Vigo, Spain
* Correspondence: adiez@uvigo.es

**Abstract:** Fluoride-doped $TiO_2$ (F-$TiO_2$) was synthesized by an efficient and simple one-step synthesis and successfully used for the UV-photo-degradation of the toxic and stable pollutants methylene blue (MB) and bisphenol A (BPA). Initially, the synthesized catalyst was characterized and compared to untreated $TiO_2$ (P25 Degussa) by different physical–chemical analyses such as XRD, band gap calculation, SEM, EDS, FITR, ECSA, or EIS. F-$TiO_2$ defeated commercial $TiO_2$, and almost complete pollutant removal was achieved within 30 min. The energy consumption was reduced as a result of the suitable reactor set-up, which reduced light scattering, and by the application of a long-pulse radiation procedure, where the lamp was switched off during periods where the radical degradation continued. This enhanced the overall photocatalysis process performance. Under these conditions, 80% of MB removal was attained within 15 min radiation with an energy consumption of only 0.070 Wh $min^{-1}$, demonstrating a much better efficiency when compared to previously reported data. The catalyst was reusable, and its performance can be improved by the addition of $H_2O_2$. The results were validated by BPA degradation and the treatment of real wastewaters with both pollutants. The results were so encouraging that a scale-up reactor has been proposed for future studies.

**Keywords:** catalyst synthesis; fluoride-doped titanium dioxide; pulse radiation; process evaluation; photocatalyst characterization

**Citation:** Díez, A.M.; Núñez, I.; Pazos, M.; M.A. Sanromán; Kolen'ko, Yu.V. Fluoride doped $TiO_2$ photocatalyst with enhanced activity for stable pollutants degradation. *Catalysts* **2022**, *12*, 1190. https://doi.org/10.3390/catal12101190

Academic Editors: Jorge Bedia and Carolina Belver

Received: 13 September 2022
Accepted: 2 October 2022
Published: 7 October 2022



## 1. Introduction

One of the main global problems is the limited access to uncontaminated water, particularly in developing countries. Among other alternatives, a promising remediation method is photocatalysis. This process is based on the action of a photocatalyst that, after being irradiated with a specific wavelength radiation, has the capacity of generating active species that decompose pollutants [1,2].

The most used photocatalyst is $TiO_2$, a well-known semiconductor that is not toxic, insoluble, cheap, and very selective on its absorption spectrum [3,4]. This last property makes $TiO_2$ very active in the UV range. $TiO_2$ commercialized from Degussa (so-labelled P25) has shown the best performance. Nevertheless, there is still room for improvement with the aim of using this process in real scenarios. Among the parameters to be optimized, there is the widening of the required radiation wavelength of activation and the inhibition of the electron-hole ($e^-/h^+$) recombination [5].

Indeed, the $e^-/h^+$ generated on the semiconductor are the responsible species for, respectively, the reduction and oxidation of pollutants and $O_2$ or $H_2O$. These cause the generation of oxidant radical species such as $HO\cdot$ or $HO_2\cdot$. $TiO_2$ has a high $e^-/h^+$ recombination rate which diminishes its degradation performance [1,4]. Consequently, several $TiO_2$ modifications have been tried in order to capture the $e^-$; hence, the

recombination rate would be reduced, providing more time for the reactions of free radical production to happen [2,3].

However, new photocatalysts usually require long and expensive synthesis processes. For instance, Zhan et al. [2] reported the application of a V/Mo-$TiO_2$ catalyst, the synthesis of which involved several steps and calcination during 4 h at 500 °C. They attained almost complete MB degradation after 1 h. In other studies, the catalyst contained expensive elements such as in the Bi/Ag-$TiO_2$ catalyst [6]. Similarly, the $WO_3$/$KNbO_3$ photocatalyst was used for attaining BPA and MB degradation within 20 min by using a 375 W UV lamp. Thus, lamp consumption and the catalyst selection increases the complexity and price of the process [7]. In fact, other authors have pointed out the necessity of more environmentally friendly synthesis processes [8].

We hereby propose a more realistic photocatalyst, where the synthesis process is simple, inexpensive, and environmentally friendly based on the single addition of an element in what we have labelled as one-step synthesis. In this context, several studies stand out, in which catalysts were synthesized by $TiO_2$ doped with graphene [9] or doped with electronegative compounds such as N, P, S, or halogens, reducing the band gap and shifting the absorption edges favoring photocatalysis [3].

Nevertheless, recent studies have demonstrated that the well-known methylene blue (MB) is still being treated by the usage of complex catalysts. For instance, Bibi et al. [10] required the addition of reduced GO and $Fe_3O_4$ to $TiO_2$ on different steps so they arrived at 99% degradation of 3 mg/L of MB effluent within 70 min. Likewise, other authors [11] made a composite Ni/$TiO_2$/zeolite by several calcination steps and even with this catalyst, they needed long treatment times (2 h) for complete MB removal. On the other hand, when the synthesis process is simpler, the MB photodegradation requires the usage of high intensity lamps [12]. In this study, the addition of fluorine to the $TiO_2$ surface, in order to avoid or retard $e^-/h^+$ recombination is reported. This catalyst is based on a previous paper about gas treatment [13] and it may also be useful for effluent treatment. Other authors have essayed the synthesis of F-$TiO_2$ throughout more complex processes, attaining good efficiencies on MB removal [14].

This one-step synthesized F-$TiO_2$ catalyst would be, for the first time, assessed for liquid effluent treatment, using two stable model pollutants, namely MB and bisphenol A (BPA). Several authors have carried out the procedure of complementing MB degradation study with a BPA plasticizer [7,15]. This procedure favors the validation of photo-based processes for the degradation of aromatic stable compounds, regardless of being colorful (MB) or colorless (BPA). Moreover, these compounds cause environmental problems due to their stability, toxicity, and increasing usage [15]. Sadly, traditional treatment alternatives such as biodegradation are not efficient for BPA and MB removal due to their stability and toxicity to microorganisms [15]. Therefore, photocatalysis has been proposed as an alternative, although the up-to-date proposed catalysts are complex and have been synthesized by environmentally unfriendly methods. For instance, the glass fibers of Fe-$TiO_2$–carbon quantum dots [4] or nanodiamond-$TiO_2$ [8] have been used for the elimination of these pollutants..

Another bottleneck in the photocatalysis processes is related to efficiency problems due to both i) light scattering with solution depth [16] and ii) high energy consumption (EC) related to the requirement for UVA lamps, as it is the most useful radiation for $TiO_2$-based photocatalysis [9].

This research attempts, for the first time, the usage of the one-step-synthesized F-$TiO_2$ on liquid stream photocatalysis. The scarce studied long-pulse procedure with the usage of a UVA-LED lamp was proposed in order to reduce EC. The $H_2O_2$ addition was also considered in order to promote higher degradation rates [17]. What is more, a novel reactor design based on the reduction in solution depth and the increase in radiated surface area was utilized, reducing light scattering. Considering this used set-up, a scale-up reactor is proposed.

## 2. Results

### *2.1. Preliminary Tests*

#### 2.1.1. Rector Set-up

To begin with, and taking into consideration the influence of the radiated area and light scattering on photo-based processes [16], the degradation of a 20 mg/L MB solution was carried out in both an open-wide reactor and a narrow-open reactor using $TiO_2$ (800 mg/L) as the model photocatalyst (Figure S1). By increasing the solution depth and reducing the radiated area, the MB degradation was reduced by 65% and the pseudo-first kinetic rate of the degradation was reduced by 10 units, that is from 0.024 $min^{-1}$ ($R^2 = 0.9970$) to 0.0027 $min^{-1}$ ($R^2 = 0.9906$).

In order to standardize the results, the EC per mg of MB was calculated following Equation (1), where L is the lamp power (W), t is the time the lamp is switched on (h), and m is the mass of the eliminated MB (mg).

$$EC\ (Wh\ mg^{-1}) = L \cdot t/m \quad (1)$$

Indeed, on the open-wide reactor, the EC was 0.154 Wh/mg, whereas the EC on the narrow-open reactor was 0.521 Wh/mg.

#### 2.1.2. Catalyst Doping Dosage

Then, the variation of catalyst performance depending on F dosage was evaluated (Figure S2). No significant differences were found when the content of $TiO_2$:F was varied from 1:0 to 1:2. The ratio of $TiO_2$:F 1:1 was selected to continue the experiences due to slightly quicker degradation kinetics. Smaller quantities resulted in a degradation profile equal to raw $TiO_2$. Thus, the F-$TiO_2$ catalyst with a ratio 1:1 was used thereafter, and it was named F-$TiO_2$.

#### 2.1.3. Catalyst Concentration

The study of the catalyst dosage was studied with the optimal F-$TiO_2$. Figure S3 depicts both the degradation profile in time and the pseudo-first order kinetic constants. As can be seen, increasing the catalyst dosage favored the degradation performance and rate until 1,600 mg/L of F-$TiO_2$ was used. Nevertheless, slight differences were found between 800 and 1,600 mg/L and, what is more, the latter exhibited 10% of adsorption, which made the actual degradation 85%, instead of 97% in the case of using 800 mg/L of F-$TiO_2$. A total of 3,200 mg/L caused 17% initial adsorption and a detriment on overall MB removal after 30 min. Consequently, 800 mg/L of F-$TiO_2$ was selected as the optimal dosage and used thereafter.

### *2.2. Characterization*

The characterization of F-$TiO_2$ was carried out and it was compared to commercial Degussa P25 $TiO_2$.

#### 2.2.1. XRD

Crystalline structures of $TiO_2$ and F-$TiO_2$ were analyzed throughout the XRD analysis. The spectra of both samples are shown in Figure S4. Typical anatase and rutile phases confirmed the stability of the $TiO_2$ sample after F doping. F content was not detected on XRD.

#### 2.2.2. Raman

Raman spectra show the characteristics peaks of anatase $TiO_2$ (Figure 1), namely those placed at 148.5 [Eg (1)], 397.5 [B1g], 516.15 [A1g], and 635.2 [Eg (2)] $cm^{-1}$ [8]. Slight differences between $TiO_2$ and F-$TiO_2$ were detected (Figure 1B) which were related to successful F doping [18].

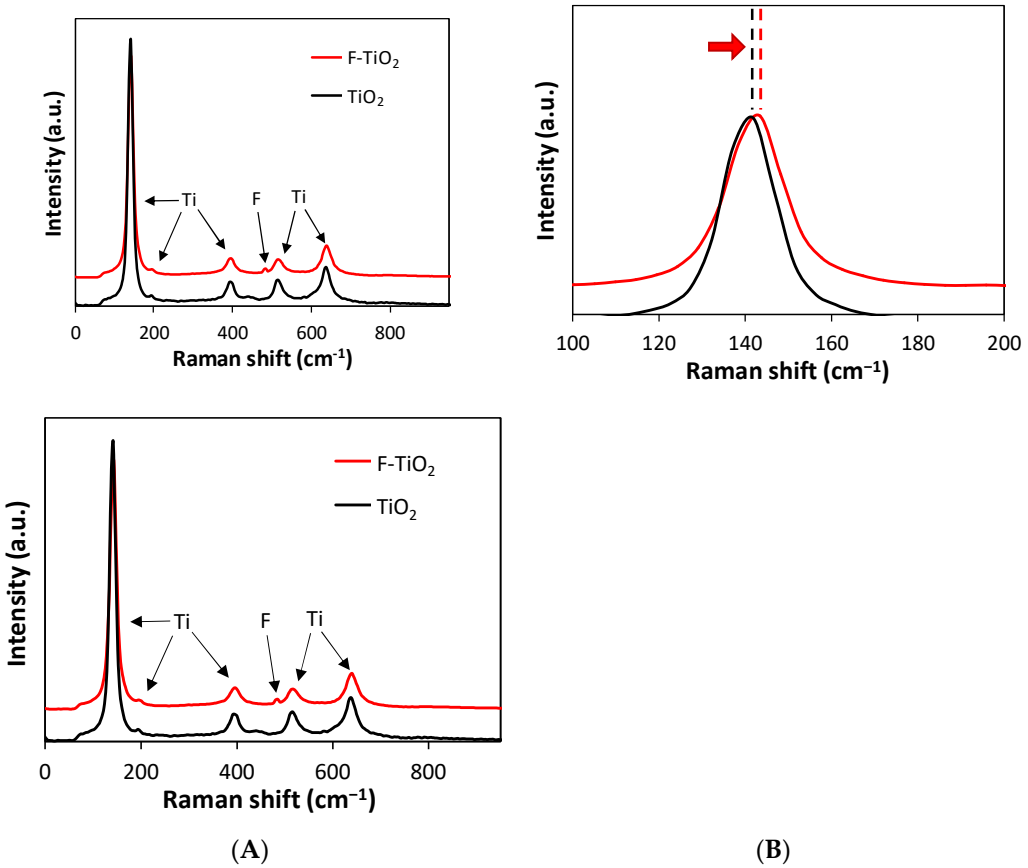


**Figure 1.** Raman spectra of F-$TiO_2$ and $TiO_2$ catalysts (**A**), zoom in on the Raman spectra in the range 100–200 $cm^{-1}$ (**B**).

2.2.3. SEM, EDS and ICP

The SEM image (Figure S5) demonstrates that the particle size was in the μm order due to the agglomeration of the particles caused by the synthesis process. A small C quantity was detected maybe due to the remaining IPA from the synthesis process. The EDS results demonstrate the successful F doping where 8% of F was detected. These data were corroborated by ICP measurements after acid digestion of the catalyst. The ICP results showed that each 0.25 mg of sample contained 0.11 mg of Ti (that would be 0.184 mg of $TiO_2$) and 0.015 mg of F.

2.2.4. UV-Vis Spectra

Spectrophotometric measurements were taken in order to evaluate the differences in the UV-Vis responses of both the $TiO_2$ and F-$TiO_2$ catalysts. The UV-Vis response was used for calculating the Tauc plots (Figure S6) following Equation (2), where v is the frequency, A is the proportional constant, n is 4 due to an indirect transition, and $E_g$ is the band energy [19]. The $TiO_2$ band gap resulted in 3.2 eV, demonstrating the high percentage of the anatase phase on commercial $TiO_2$ (the rutile phase had a band gap of 3 eV) [3]. On the other hand, F-$TiO_2$ provided a band gap of 1.5 eV, demonstrating that the addition of F narrowed the band gap of $TiO_2$.

$$h\upsilon \cdot \alpha = (Ah\upsilon \cdot E_g)^{n/2} \quad (2)$$

2.2.5. Electrochemical Measurements

The electrochemical performance of materials has been demonstrated to be related to their photo-catalytic performance, as it is indicative of electron mobility (Electrochemical Impedance Spectroscopy: EIS) [20] and active surface area (ECSA) [19].

EIS

EIS results are provided in Figure 2, where the equivalent circuits are depicted. The series resistance represents the electrode [21]; this is why the values were practically constant (14.9 and 12.4 Ω), as in both cases Ni-Foam was the supporting working electrode. The parallel resistance stands for the layer resistance of the material [21], and in this case F-$TiO_2$ provided a much smaller value than $TiO_2$ (1.77 vs. 12.5 kΩ), demonstrating the electron mobility was much higher on F-$TiO_2$ [20], which may be related to better photocatalytic activity.

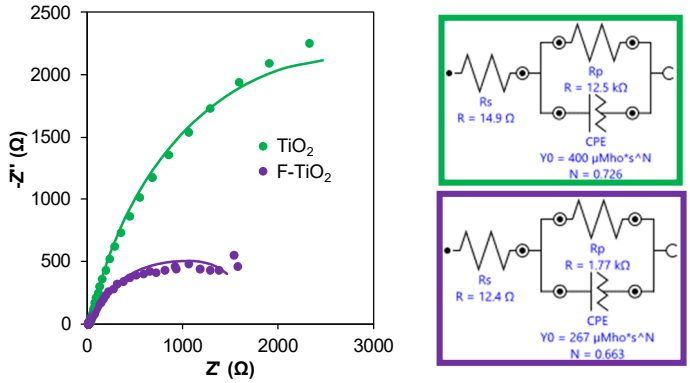


**Figure 2.** EIS measurement of $TiO_2$ (green) and F-$TiO_2$ (purple) with the fitting of the equivalent circuits.

ECSA

ECSA is also related to catalytic activity [22]. After the representation of CVs regarding the scan rate (Figure S7) and following Equation (3), CDL was 0.3 and 0.2 uF $cm^{-2}$ for F-$TiO_2$ and $TiO_2$, respectively. That means the ECSA values were 7.5 $cm^2$ and 5 cm, respectively. Therefore, the surface area useful for electrochemical reactions was 30% higher in the case of F-$TiO_2$.

*2.3. Pollutant Abatement*

Subsequently, the degradation of the model pollutant MB was carried out, and different parameters were considered.

2.3.1. Catalyst Evaluation

The comparison of synthesized F-$TiO_2$ with commercial $TiO_2$ on the performance of MB degradation was accomplished on the wide-open reactor (Figure S2). The results manifest the suitability of the reactor set-up and the efficacy of $TiO_2$ to work as UV-photocatalyst, as in both cases more than 80% degradation was attained within half an hour. Moreover, the higher performance of F-$TiO_2$ was remarkable; after the one-step synthesis, it provided an extra 25% MB elimination. Indeed, the pseudo-first order kinetic values also denote a much higher efficiency of F-$TiO_2$ vs. $TiO_2$ being, respectively, 0.1367 $min^{-1}$ and 0.0220 $min^{-1}$. The usage of this one-step synthesized photocatalyst also favored the efficiency of the process as the EC was 0.152 and 0.121 Wh $mg^{-1}$ for $TiO_2$ and F-$TiO_2$, respectively, demonstrating the efficacy of the latter.

The high efficiency of the F-$TiO_2$ catalyst was not only demonstrated by its comparison to the well-performant $TiO_2$, but also to previous recent data (Table 1). The high complexity of the synthesis processes is remarkable.

**Table 1.** Last reported data on MB and BPA UV-photocatalysis degradation.

| MB (mg/L) | Catalyst (mg/L) | Lamp (nm, w) | Time (min) | Degradation (%) | EC (W·h/mg) | Reference |
|---|---|---|---|---|---|---|
| 20 | F-$TiO_2$ (800) | 360–365 nm, 4.8W | 15 | 78.84 | 0.070 | This study |
| 20 | F-$TiO_2$ (800) | 360–365 nm, 4.8W | 30 | 96.24 | 0.121 | This study |
| 73.57 | Graphene-$TiO_2$ (50) | 360 nm, 17 W | 480 | 87 | 2.12 | [9] |
| 10 | F-$TiO_2$ (200) | 300 W | 20 | 88 | 11.25 | [14] |
| 5 | GO-$TiO_2$ (200) | 500 W | 60 | 92 | 108.7 | [1] |
| 3.2 | V/Mo-$TiO_2$ (1000) | 365 nm, 8 W | 60 | 86.7 | 2.88 | [2] |
| 10 | Zeolite/Ni-$TiO_2$ (50) | UV, 16 W | 120 | 100 | 3.20 | [11] |
| 10 | $TiO_2$ nanoparticles (60) | UV, 300W, >420 nm | 24 | 99 | 12.12 | [12] |
| 10 | $WO_3$/$KNbO_3$ (3000) | 365 nm, 375 W | 40 | 98 | 24.3 | [7] |
| 3 | rGO-$Fe_3O_4$/$TiO_2$ (150) | UV, 500 W | 70 | 99 | 196.4 | [10] |
| **BPA (mg/L)** | **Catalyst (mg/L)** | **Lamp (nm, w)** | **Time (min)** | **Degradation (%)** | **EC (W·h/mg)** | **Reference** |
| 20 | F-$TiO_2$ (800) | 360–365 nm, 4.8W | 30 | 98 | 0.122 | This study |
| 10 | $WO_3$/$KNbO_3$ (3000) | 365 nm, 375 W | 240 | 49 | 300 | [7] |
| 10 | Nanodiamond-$TiO_2$ (80) | UV, 20 W | 100 | 96 | 3.47 | [8] |
| 20 | Glass Fibers Fe-$TiO_2$-carbon quantum dots (n.r.) | $\lambda$ < 472 nm, 55 W | 60 | 100 | 2.75 | [4] |
| 20 | ZnO-Graphene oxide | 254 nm, 15 W | 60 | 99.5 | 0.75 | [23] |

n.r. = not reported.

### 2.3.2. Long-Pulse Radiation Procedure

Taking into consideration the fact that photocatalysis degradation is a radical attack, we considered the poorly studied possibility of treating the effluent by alternating radiated and dark periods. That is, we proposed the usage of the lamp in the long-pulse radiation procedure, so the lamp consumption could be reduced for future usages. In this procedure, the lamp was switched on from 0 to 5 min treatment time and from 10 to 20 min of treatment time. As it can be seen in Figure 3, after 10 and 30 min the detriment on MB degradation was only, 20 and 10%, respectively, whereas the lamp usage was reduced to a half. This means that EC was reduced, roughly, to a half (Figure 3). Consequently, the EC for MB degradation within 30 min was 0.070 Wh $mg^{-1}$ with the long-pulse radiation procedure.

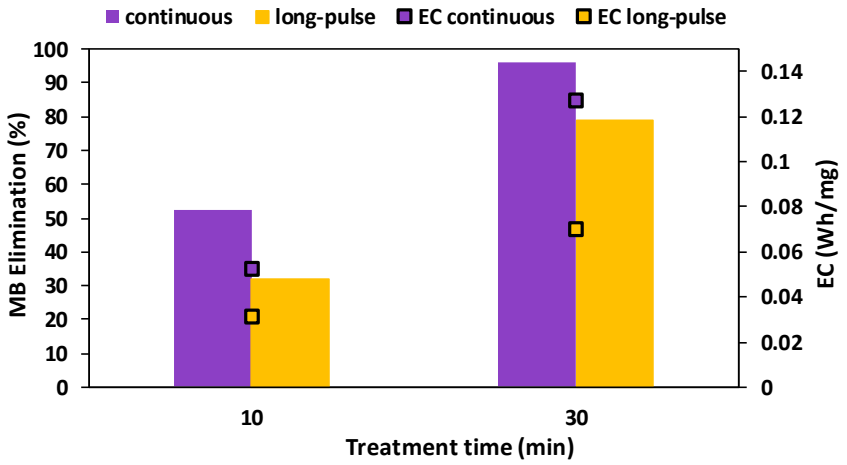


**Figure 3.** MB elimination (20 mg/L) at a catalyst concentration of 800 mg/L. Continuous radiation (purple), and long-pulse radiation (yellowish).

2.3.3. Reusability

Evaluating the reusability of the catalyst is mandatory for future applications [19] and thus, it was evaluated. For practical purposes, the experiences were tested with continuous radiation. First of all, the reutilization of F-$TiO_2$ led to a 17% detriment on the third cycle (Figure 4A) which is within typical values [19]. Samples were filtered by 0.22 μm and measured by ICP, where F and Ti content was below detection limits, demonstrating that the doping process is not only simple and economic, but also efficient, leading to a stable F-$TiO_2$ photocatalyst.

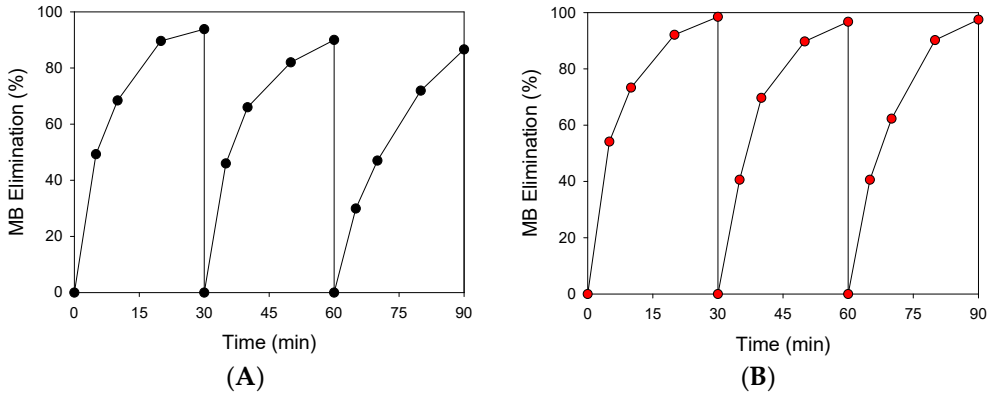


**Figure 4.** MB elimination (20 mg/L each cycle), using the same photocatalyst in three cycles (800 mg/L) (**A**). MB elimination (40 mg/L each cycle), using the same photocatalyst in three cycles (800 mg/L), and adding 0.3 mg/ml of $H_2O_2$ (**B**).

Nevertheless, the addition of $H_2O_2$ as an extra oxidant has been reported to favor photocatalysis [17] and hence, the addition of 0.3 mg/mL of $H_2O_2$ in each cycle was evaluated (Figure 4-B). Indeed, the process was so favorable that 40 mg/L of MB was used in order to have enough room for improvement as well as a better quantification (20 mg/L was eliminated too quickly). One can compare Figures 4-A and 4-B and the detriment detected on the degradation of 20 mg/L of MB without $H_2O_2$ (Figure 4-A) was not detected when $H_2O_2$ was added, even though the initial MB concentration was 40 mg/L (Figure 4-B). In any case, the MB concentration effect is studied in next section in order to compare the results with these data.

2.3.4. Pollutant Concentration

The effect of MB concentration was then studied (Figure 5). When the initial MB concentration was set at 40 mg/L, the degradation plunged to 50% (Figure 5A). Concentration differences were more significant during the first 10 minutes of radiation (Figure 5B) where one can notice that the MB degradation was practically constant in the range 5–20 mg/L, whereas the performance abruptly decreased at 40 mg/L. With 0.3 mg/L of $H_2O_2$, this detriment did not take place and, what is more, the catalyst could be reused for up to three cycles (Figure 4B).

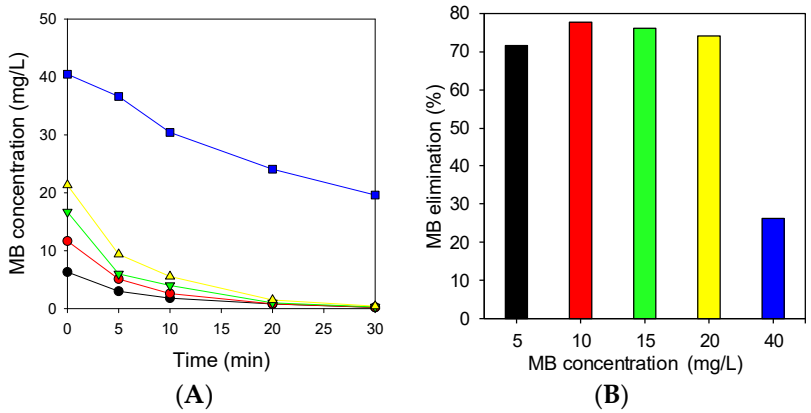


**Figure 5.** MB degradation under UV radiation depending on the initial MB concentration (**A**). MB degradation after 10 min treatment (**B**).

2.3.5. Treatment of More Complex Effluents

Then, the photocatalyst and reactor set-up suitability for the treatment of polluted effluents were corroborated by treating a solution with the complex polymer BPA as well as real wastewaters with both MB and BPA (Figure 6). This procedure allows the suitability of this process with colorful and colorless effluents to be confirmed. Both pollutants suffer photocatalytic degradation, which is started by the radical attack, so hydroxylation occurs in areas close to the aromatic ring, which are electronegative. Then, the scission of the ring takes place, liberating some carbonaceous chains which end up on simple carboxylic acids [24,25].

Regarding MB degradation (Figure 6-A) the efficiency was reduced (30%) when using real primary-treated wastewater, contrasting with the results using the distilled Milli-Q matrix. Moreover, when using secondary wastewater, the result was slightly better due to the reduction of the organic matter due to the biological degradation (Table S1). The total organic carbon (TOC) of the solution was 13 mg/L when MB was dissolved in Milli-Q water and 86% mineralization was attained within 30 min of photocatalysis. At this point, the remaining carbon was related to carboxylic acids, which reduced the solution pH from 5.8 to 5.4. On the other hand, the presence of a more complex wastewater matrix increased the initial TOC to 91 and 54 mg/L for, the primary and secondary-treated wastewaters, respectively. After the photodegradation process, TOC was reduced by 66 and 71%, respectively, and the pH was reduced by 0.2 units in both cases. This demonstrates there acid intermediates were also generated although the pH drop was smaller due to the buffer behavior of the salt content (both samples had high conductivity: Table S1). Moreover, the remaining TOC was related to the MB molecule, which was not completely removed due to the degradation of the organic matter already present on the real wastewaters.

Regarding the pseudo-first order kinetic adjustment (Table S2), the slope was around 0.13 $min^{-1}$ for MB treatment on real wastewaters due to the increased complexity of the effluent, as the constant rate was 0.137 $min^{-1}$ when treating MB in Milli-Q water.

Figure 6B demonstrates the suitability of the degradation process for different stable and toxic pollutants, as even BPA was almost completely removed within 30 min. In this case, the treatment of BPA in a primary or secondary wastewater also caused a detriment of around 20% on the performance of the photocatalysis process. In this case, mineralization on Milli-Q water achieved 83% in 30 min and the pH was reduced from 6 to 5.4, which may have been due to the generation of more carboxylic acids, as the BPA-Milli-Q solution had an initial TOC of 16 mg/L. In the case of treating real wastewaters, mineralization dropped to 69 and 76%, for, primary and secondary-treated wastewaters, respectively. This demonstrates that BPA degradation was easier than in the case of MB, due to the fact BPA and its by-products do not cause light scattering. In this case, the pH dropped by 0.4

and 0.3 units, respectively, demonstrating the generation of carboxylic acids [25]. Further studies need to be completed on the scale-up study of this process.

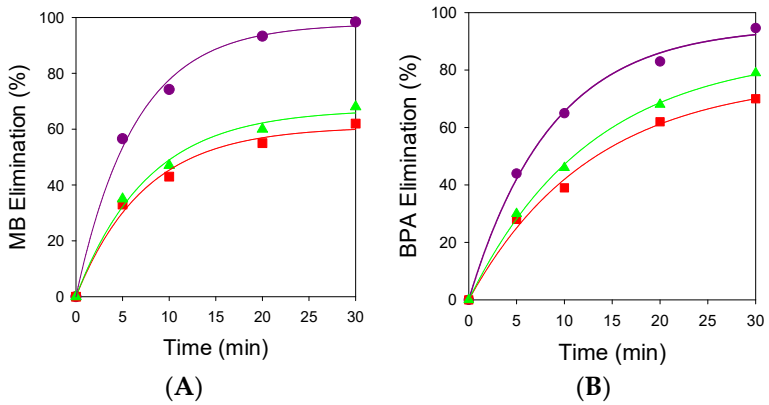


**Figure 6.** MB (**A**) and BPA (**B**) elimination (20 mg/L) at a catalyst concentration of 800 mg/L with pseudo-first order kinetics adjustment (line) in wastewater that just received a primary treatment (red squares), that received a secondary treatment (green triangles), and Milli-Q water (purple circles).

## 3. Discussion

In order to understand the efficiency of the proposed process, specifically in terms of photocatalyst activity and reactor set-up, some previous studies depicted on Table 1 were used as references and are commented on throughout this section.

### *3.1. Preliminary Tests*

#### 3.1.1. Reactor Set-up

The preliminary test for the MB degradation with $TiO_2$ photocatalysis was completed. With the $TiO_2$ catalyst, the comparison between the performance of the wide and the narrow-open reactors (Figure S1) demonstrated the degradation was improved when (i) the solution depth was smaller and (ii) when the radiation area was bigger (open-wide reactor: Figure 7) due to a better activation of the photocatalyst and a reduction in the light scattering. This reactor is notably thinner than the typical cylindrical reactor and moreover, it has the radiation source placed at 3 cm from the solution. Jafari et al. [4] also placed their lamp at 3 cm for BPA degradation; however, their reactor was 5 cm in diameter and 10 cm in height, producing an elevated light scattering, which may cause a lower efficiency than the hereby attained value (2.75 vs. 1.22 Wh/mg, respectively). In fact, they required twice the time for achieving the same degradation of 20 mg/L of BPA (Table 1).

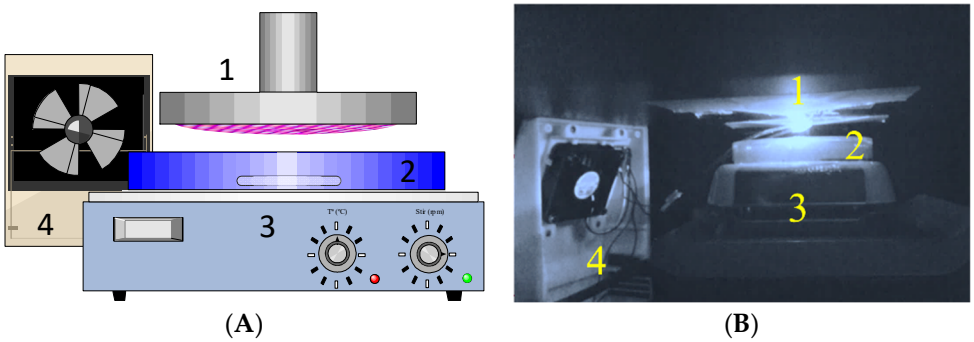


**Figure 7.** Reactor set-up, schema (**A**), and real (**B**): UV LED (1), crystal open-wide-reactor (2), magnetic stirrer (3), and refrigerator fan (4).

The EC attained in this study was smaller than most of previous references (Table 1). This may indicate, apart from a proper photocatalyst selection, the suitability of the reactor set-up. Indeed, several authors have reported the positive effect of reducing the treated effluent depth when working with photocatalysis systems [26]. Hence, Shiraishi et al. [16] concluded that the UV intensity received on the photocatalyst decreases as liquid depth increases. Nevertheless, they highlighted that the negative effect of solution depth can be overcome with high mixing. In fact, a smaller solution depth reduces light scattering [6]. In our study, the good results may have been fomented by a small solution depth, an elevated radiated area, and a high mixing rate. For instance, Zhang et al. [2] attained an extremely high EC (Table 1). These authors may also have used an elevated catalyst concentration (1000 mg/L) of the complex V/Mo-$TiO_2$ catalyst. This might have produced light scattering, making the catalyst activation difficult. In fact, these authors used a reactor set-up with ian nappropriate photo-activation, as the lamp was placed at 8 cm instead of the 3 cm fixed in this study. Moreover, the sample was placed in a beaker which undoubtedly has a smaller width than the open-wide reactor hereby proposed (Figure 7). These authors may have attained higher efficiencies by the utilization of a wide-open reactor and higher stirring rates.

Another example was brought by Niu et al. [12] who placed the lamp 15 cm above of the sample, increasing the EC to 12.12 Wh $mg^{-1}$. Both results could have been promising if the lamp was placed closer to the sample, as the intensity of the lamp is reduced exponentially with distance from the source [27,28]. Indeed, the catalytic performance is related to photo-current intensity, as a greater intensity engenders more $e^-/h^+$ pairs due to the generation of easier electron transitions [12]. Considering the results attained in this research study, a new reactor set-up is proposed (Figure S8), based on the proximity of the radiation source from the bulb solution and the reduction in solution depth.

#### 3.1.2. Catalyst Doping Dosage

Different F dosages were evaluated (Figure S2), namely, $TiO_2$:F ratios of 1:0.5, 1:1 and 1:2 as other authors noticed differences related to the performance of UV photocatalysis related to the doping dosage [23,29]. Considering the slight differences, the most efficient photocatalyst to work with was $TiO_2$:F 1:1 which was further characterized and compared to commercial $TiO_2$. The exact amount of F dopant was evaluated by subsequent ICP and EDS.

#### 3.1.3. Catalyst Concentration

The effect of photocatalyst dosage was in concordance with previous authors. Thus, a lack of catalyst amount prevents the availability of active sites to be activated by irradiation, whereas an excess of photocatalyst causes the agglomeration of the particles and light scattering [10,30]. This was clearly noticed when testing 3,200 mg/L of F-$TiO_2$ (Figure S3) where the performance was similar to that of 800 mg/L until it reached 20 min of treatment time. Indeed, after 20 min the performance was even reduced which may be consistent with the excessive generation of oxidants which react with themselves due to a lack of MB particles (as the initial concentration was diminished due to degradation) [31]. Likewise, Bibi et al. [10] demonstrated that MB removal increased from 60 to 100% when switching the rGO-$Fe_3O_4$/$TiO_2$ catalyst concentration from 50 to 150 mg/L. Oppositely, increasing their photocatalyst dosage to 200 mg/L led to a 15% detriment in relation to MB elimination. In our study, slight differences were found between the 800 and 1,600 mg/L catalyst dosage, although considering the economic aspects and the fact that 1,600 mg/L overestimated the degradation performance due to adsorption, 800 mg/L was selected as the preferred concentration.

### *3.2. Characterization*

#### 3.2.1. XRD

XRD spectra (Figure S4) showed the characteristics peaks of anastase $TiO_2$ at 25.2º, 37.9°, 47.8°, 54.3°, and 62.7° θ, which correspond to the planes (101), (004), (200), (105), and (204), which is the most photo-active phase of $TiO_2$ [6]. Both $TiO_2$ and F-$TiO_2$ samples provided a similar XRD profile. This was caused by the fact the ionic radii of F and O are practically the same (0.133 and 0.132 nm) [32]. Moreover, the analogous XRD profiles of both $TiO_2$ and F-$TiO_2$ demonstrated that the synthesis process at low temperatures and atmospheric pressure is considerate of the $TiO_2$ crystalline structure.

#### 3.2.2. Raman

Raman spectra of $TiO_2$ and F-$TiO_2$ (Figure 1) demonstrated that $TiO_2$ was chemically stable in the synthesis process as the spectra were mainly constant. However, F addition caused a defect introduction at 490 $cm^{-1}$ which can be related to F content [33]. The characteristic peak of Ti at 148.5 $cm^{-1}$ suffered a shift and a peak broadening (Figure 1B) due to the formation of F-Ti-O [18].

#### 3.2.3. SEM and EDS

The particle agglomeration (Figure S5) on the F-$TiO_2$ catalyst can be positive for the photocatalysis performance [8]. EDS provided the experimental weight ratio Ti:F of 8.25:1 which would be an atomic ratio of 3.3:1. The ICP results showed the actual atomic ratio of Ti:F was 2.8:1. These slight differences can be explained by the superficial character of the EDS measurement.

#### 3.2.4. UV-Vis Spectra

The fluoride doping caused an increase in the solar spectrum [3] as can be seen in Figure S6, where the band gap of F-$TiO_2$ was 1.5 eV vs. the 3.2 of commercial $TiO_2$. This was caused by the addition of F, which adds defects that not only reduce the band gap but also act as active centers [2]. Consequently, visible radiation absorption is favored as well as UV absorption [14]. In fact, several authors have demonstrated the dual UV and visible activity of their synthesized catalysts such as V/Mo-$TiO_2$ [2] or $TiO_2$-$SiO_2$ [34]. This dual activity needs to be corroborated in future studies with F-$TiO_2$.

By doping $TiO_2$, electron trapping is favored and thus $e^-/h^+$ recombination is diminished [3] which is related to a better photocatalysis performance. This electron trapping may be favored by electronegative compounds such as F.

#### 3.2.5. Electrochemical Measurements

EIS

The smaller radius arc of the F-$TiO_2$ sample when compared to $TiO_2$ (Figure 2) is related to a better charge transfer and to a lower $^-/h^+$ recombination [20,35]. The linear part of the Nyquist plot (0–200 Ω of real Z) is proportional to the limited diffusion processes [36]. Consequently, the fact that the slope is less blatant for F-$TiO_2$ indicates that this catalyst favors a better diffusion when compared to commercial $TiO_2$. Indeed, the wider semicircle on the $TiO_2$ catalyst indicates the electrons reach the semiconductor/interface where the photocatalysis occurs with more difficulty, and thus these electrons could recombine with holes before reacting with pollutants or oxygen molecules [20]. This high charge separation and conductivity of F-$TiO_2$ indicates it would act as a better catalyst [36]. Indeed, a lower resistance, which is related to a faster migration of electrons and holes, has been associated with a higher generation of radicals throughout the degradation process. This lower resistance enhances the photocatalytic activity so the pollutant can be degraded [12]. Other authors have demonstrated a better charge separation efficiency by the attainment of smaller arc radius [37].

ECSA

Active surface area controls the activity of the photocatalysts due to the interaction between the pollutant and photocatalyst. Indeed, a higher ECSA implies an increased adsorption of the target compound due to the presence of a higher surface area as well as the presence of more active sites [19]. Thus, higher ECSA values favor photodegradation processes [22,38]. In fact, the higher ECSA of F-$TiO_2$ (Figure S7) demonstrated that this catalyst favors light capture, carrier separation, and transfer ability [22].

### *3.3. Pollutant Abatement*

#### 3.3.1. Catalyst Evaluation

The performance enhancement can be explained by the reduction in the $e^-/h^+$ recombination caused by the substitution of F with O atoms in $TiO_2$, forming a Ti-F bond. These Ti-F bonds have a higher $e^-$ attraction and the $e^-/h^+$ recombination is more difficult [3]. This is probably due to the strong F electronegativity. This provides extra time for the electrons to react to produce radicals involved in the pollutant's degradation [39].

These EC results were considerably smaller than the previously reported data (Table 1). Other authors have used inefficient photocatalyst and reactor set-ups which they have tried to overcome by the utilization of elevated consumption lamps. For intance, Badvi and Javanbakht [11] were far from our one-step-synthesis of the catalyst; indeed, they needed calcination steps (which increase the operational costs) and several sol-gel reactions. However, 2 h was necessary for complete MB degradation and the efficiency was 23 and 41 times lower than in the case of using our F-$TiO_2$ process under continuous radiation or the long-pulse procedure, respectively. It is remarkable that these authors used 1,000 mg/L of the initial catalyst concentration which may have had a detrimental effect (Section 3.1.3).

In general, the appropriate photocatalyst selection, reactor, and lamp configuration decreased the EC. This is discussed in the last section (Section 3.3.6).

#### 3.3.2. Long-Pulse Radiation Procedure

This novel set-up was extremely efficient (Figure 3); indeed, the F-$TiO_2$ system required 0.125 Wh $mg^{-1}$ for the degradation of MB, which would mean a cost of $2 \times 10^{-5}$ EUR/$mg^{-1}$ using the actual energy cost in Spain. Considering the long-pulse procedure, the EC was reduced to 0.070 Wh $mg^{-1}$ ($1.1 \times 10^{-5}$ EUR/$mg^{-1}$) demonstrating the suitability of this procedure on radical-based processes. With this lower EC, the application costs of this process would be proportionally lower. In fact, the results of radiation on switch on/off mode were in concordance with some studies where the switching off of the lamps did not cause a direct elimination of the current response, demonstrating the presence of $e^-$ and $h^+$ [28,37].

The suitability of the reactor set-up, the efficiency of the photocatalyst, and the possibility of working with radiation on long-pulses increased the efficiency of the process when compared with recent studies (Table 1).

For instance, Gao et al. [14] reduced both the initial concentration and the treatment time to 20 min. Nevertheless, the EC was extremely high due to the usage of a high consumption lamp (300 W). These authors could have reduced EC roughly to a half by using the long-pulse procedure and probably by selecting a higher efficient photocatalyst.

#### 3.3.3. Reusability

F-$TiO_2$ showed a high reusability performance (Figure 4) due to the F doping which reduces the transformation from anatase to rutile phases, making it more stable throughout the degradation process [3]. The slight reduction in performance meant the generated by-products did not block significantly the active sites of the catalyst [2]. Moreover, considering no Ti nor F were detected after three degradation cycles, one can conclude the F-$TiO_2$ synthesis provides a stable and well-performant catalyst.

Nonetheless, the reusability was assessed with the presence of $H_2O_2$, and consequently, the degradation performance was kept constant during three batches even at double MB initial concentration. This was due to the fact the F-$TiO_2$ catalyzes the decomposition of $H_2O_2$ into HO· radicals [11] and thus, the presence of an additional amount of radicals make the process more performant. Moreover, $H_2O_2$ acts as electron acceptor, avoiding $e^-/h^+$ recombination [11]. This result confirms that $H_2O_2$ is a powerful substance that can prolong the life of a catalyst and can burst this process.

#### 3.3.4. Pollutant Concentration

Initially, the influence of MB concentration was tested so the process was validated to work with concentration variations. The process was stable at around 85% degradation in 30 min at concentrations between 10 and 20 mg/L (Figure 5). Nevertheless, reducing the concentration to 5 mg/L caused an MB degradation of 75%. This can be explained by the fact that too few pollutant molecules make the oxidant species react between themselves, losing effectivity [31]. Indeed, other authors reported a lower degradation of MB when its initial concentration was reduced [40,41]. On the other hand, increasing the concentration to 40 mg/L reduced MB elimination to 52.4%. Other authors such as Chakinala et al. [6] reported this behavior. Indeed, they suffered a reduction in dye degradation of around 30% after increasing its concentration from 10 to 45 mg/L.

In the case of Kurniawan et al. [1], 30% of MB degradation detriment was attained when switching the initial concentration from 5 to 25 mg/L. This was caused by i) the radiation diffraction due to the effluent darkness, impeding photocatalyst activation [1,6], ii) the clogging of the photocatalyst surface hindering F-$TiO_2$ activation [11], iii) the excessive amount of molecules which, after being in radical state due to the photocatalysis process, react with themselves instead than with oxidants, stopping chain radical reactions, and iv) the higher amount of generated by-products which compete with the target pollutant for the active sites of the photocatalyst [4].

In all cases, the process goes slower as time passes, for instance from treatment time 20 min, the rate is much slower. This is explained by the fact that small by-products generated due to MB degradation act as radical scavengers [6]. Acosta-Esparza et al. [9] required up to 8 h to treat a quite concentrated MB effluent, and consequently, the EC increased (Table 1). Considering our data, reducing the initial concentration could have reduced the treatment time.

#### 3.3.5. Treatment of More Complex Effluents

As was reported on Figure 6, MB and BPA degradation was achieved within 30 min. This defeats previous studies (Table 1) and demonstrates the efficiency of the process, as for instance, BPA natural degradation takes 90 years [4].

Nevertheless, the slower BPA degradation rate at the beginning of the process when compared to MB degradation is significant (Figure 6 and Table S2). This could be due to the non-polar character of BPA which makes both aqueous solubilization and oxygen radical attack more difficult. Nevertheless, as treatment time passed, degradation rose due to the simpler structure of BPA when compared to MB (graphical abstract), which meant that almost complete degradation in both cases was achieved within 30 min.

The degradation of both MB and BPA was essayed on real wastewaters after primary and secondary treatment. In this case, both pollutants suffered a reduction in degradation performance due to the higher complexity of these matrixes (Table S1). Nevertheless, the results were promising and considering the detriment was less than 40% in MB and less than 30% in BPA treatment, it can be concluded that this process copes better with matrix variations than those offered in other studies. This adaptability might be due to the optimized reactor set-up and the selection of an active photocatalyst.

For instance, Jafari et al. [4] suffered a 40% detriment on 20 mg/L BPA degradation when switching from distilled water to real wastewater. Likewise, Murcia et al. [42] experienced a detriment of more than 60%, as MB was completely degraded in 2 h by $TiO_2$

when using distilled water as a matrix and in 5 h when treating a real sample collected from a handicraft factory. This may have been caused by the increased turbidity and the presence of other organic and inorganic content which consume the oxidant species available on the system and poison the photocatalyst surface due to adsorption into it [4,42].

Considering our results (Section 2.3.3), the addition of 0.3 mg/mL of $H_2O_2$ could favor the photocatalyst performance even on these complex cases, and consequently further research should focus on the addition of this oxidant and its concentration optimization. For instance, when $H_2O_2$ was added to the 20 mg/L MB photocatalytic degradation, mineralization increased from 86% to 94% when Milli-Q water was used as a working matrix. Consequently, the results demonstrate that this process could be applied as a post-treatment for real wastewaters, although $H_2O_2$ addition or longer treatment times may be necessary [4].

#### 3.3.6. Comparison with Previous Studies

The reported results highlight the high efficiency of the set degradation process. Namely, the high performance of these data can be explained by the proper photocatalyst selection and reactor set-up, as well as the consideration of the long-pulse radiation or $H_2O_2$ addition.

As it can be seen in Table 1, the synthesized F-$TiO_2$ photocatalyst performed better than others reported in the literature, or at least, more efficiently. Indeed, other authors reached quite high MB degradation rates [1,14,34]. Nevertheless, high energy expenditure lamps (order of hundreds of watts) or long treatment times were required. For example, the EC attained by Kurniawan et al. [1] was extremely elevated due to the high power lamp utilized (500 W) and the fact that in this case the treated effluent had only 5 mg/L of MB concentration, a fact than could also have caused a slight reduction in the degradation performance (Figure 5). Likewise, Acosta-Esparza et al. [9] required 8 h for almost 90% MB degradation. This could be explained by the high initial MB concentration used by those authors (Table 1). Indeed, even in our case, increasing the MB concentration from 20 to 40 mg/L led to an MB degradation switch from 88 to 52.4% in 30 min (Figure 5).

Moreover, it should be noted that it is extremely important to stop the photocatalysis process at the optimal treatment time in order to have a more efficient output. Thus, adsorption and biological or other oxidation processes (Fenton, ozonation, electrolysis, etc.) could be coupled as final polishing [43]. For instance, Gao et al. [14] achieved quite a low efficiency due to the usage of an extremely powerful lamp. However, if they had stopped the treatment time after 10 min (80% of MB degradation), the EC would have been reduced to a half (6.25 Wh/mg). Another example was brought by Badvi and Javanbakht [11] who required 2 h for complete MB degradation. Nevertheless, approximately 90% was attained in 40 min. By stopping the photodegradation process at that point, the energy expenditure would drop from having an EC of 3.2 to 1.19 Wh/mg. Those alternatives may be suitable as it has been reported that the by-products above 80% degradation are mainly simple carboxylic acids which are bio-degradable [24].

The attained EC values are related to the future application costs of these processes, and consequently, it seems the proposed catalyst and set-up could be scaled-up in further studies (Figure S8). In fact, Pham et al. [44] scaled-up the photodegradation of 20 mg/L of MB with $H_2O_2$ and even though their lamp consumed much more (25 W) than the used here (4.8 W), they established an energy cost of 8.41 EUR/$m^3$ which is competitive with other treatment processes. Our process may reduce those costs considering our degradation rate of 0.1367 $min^{-1}$ defeated the degradation rate of Pham et al. [44] (0.0105 $min^{-1}$). Indeed, the energy costs for the proposed system of 50 mL with the long-pulse procedure radiation would be 9.6 EUR/$m^3$ which, as it was reported in Section 3.3.3, could be improved with the addition of $H_2O_2$ [44].

As was described in the previous section, under the worst case scenario the performance can be enhanced by the addition of $H_2O_2$ (Figure 4B). With that, EC is controlled, as when the treatment time increases, the EC consumption increases more dramatically if

the pollutant is being degraded slowly. As an example, in this study the EC for the degradation of 20 mg/L MB was 0.093 Wh/mg after 20 min, whereas at 30 min it was 0.125 Wh/mg (and the MB degradation only switched from 82 to 94%). In Figure 3 one can see how the efficiency of the process was reduced with time, which demonstrates it is not worth increasing the treatment time; thus, adding $H_2O_2$ may be a good alternative (Figure 4B).

The good performance attained by Garg et al. is remarkable [23]. Those authors attained a small EC due to the usage of a low-consumption UVC lamp and an increase in the irradiated surface area. Nevertheless, the effect of the adsorption on their ZnO-graphene oxide catalyst should be considered, as it adsorbed around 20% of BPA. This may make the reutilization of the catalyst difficult, which was not assessed.

In general, the proposed set-up and photocatalyst are suitable for stable and threatening pollutants. Consequently, more studies should be carried out in order to complete this study, i.e., the optimization of $H_2O_2$ dosage and treatment time, in order to scale-up the process (Figure S8), fixing properly the residence time.

## 4. Materials and Methods

### *4.1. Reagents*

Titanium dioxide ($TiO_2$) Aeroxide P25 was bought from Acros Organics (Madrid, Spain); nitric acid ($HNO_3$), 70%, from Fischer Chemical (Madrid, Spain); sodium fluoride (NaF) >99%, from Sigma-Aldrich; and isopropyl alcohol (IPA) ($C_3H_8O$), from Honeywell (Madrid, Spain), as well as the ethanol (EtOH) (>99.8%). Nafion was acquired from Sigma-Aldrich (Madrid, Spain). MB (>82%) was purchased from Sigma-Aldrich. The water was supplied by a Milli-Q system (Advantage A10, from Merck, Darmstadt, Germany).

### *4.2. Catalyst Synthesis*

The synthesis was adapted from Shayegan and co-workers [13]. Briefly, 3 g of NaF was added to 230 ml of IPA, and placed on a magnetic stirrer (approx. 700 rpm) for 2 h at room temperature. Next, 0.2 M nitric acid was added until pH ≈ 3.5. After that, $TiO_2$ was added to the solution at different $TiO_2$:F ratios of 1:0.5, 1:1, and 1:2. The stirring was continued for another 3 h. During that time, nitric acid should be added to keep pH ≈ 4, if needed. When the time was finished, the obtained substance was centrifuged and washed several times, until it acquired a homogeneous color. It was dried in an oven at 100 °C for at least 12 h so F-$TiO_2$ with a molar ratio (Ti:F 1:1) catalyst was attained. Different $TiO_2$:F contents were essayed and for that, instead of 3 g of NaF, 1.5 or 6 g was used so F-$TiO_2$ was attained with a ratio of Ti:F of1:0.5 and 1:2, respectively.

### *4.3. Reactor Set-up*

The photocatalytic performance was evaluated on a novel open-wide reactor which was cylindrical with a diameter of 8 cm and a height of 3 cm. It promoted photocatalyst activation by the lamp placed 3 cm above (Figure 7) and reduced light scattering due to solution depth. Indeed, another narrow-open reactor (4 cm diameter, 10 cm height) was also evaluated with comparative aims. In both cases, magnetic sitting at 800 rpm was set. Under this stirring and in dark conditions, 30 min was left to attain the adsorption equilibrium which may take place between the catalyst and pollutant. The lamp used was a low-consumption UV-LED lamp (365 nm, 4.8 W, 78 CMF-AR-A03, from Seoul Viosys, Gyeonggi-do, Republic of Korea) and it had a small fan in order to keep the temperature constant at 22 ± 2 °C, so evaporation of the sample was avoided.

During the long-pulse radiation procedure, the lamp was switched on from 0 to 5 and from 10 to 20 min treatment time, whereas from 5 to 10 and 20 to 30 min the reaction continued in dark conditions. That meant 15 min radiation time out of 30 min of overall treatment time.

Unless stated differently, 50 mL was used and the catalyst concentration was set at 800 mg/L and the initial MB or BPA concentration was fixed at 20 mg/L, values found in real landfill leachates [4]. All experiences were performed using Milli-Q water as the working matrix (Sartorious, Göttingen, Germany). However, validation experiences were performed with real wastewater, kindly donated by WTP (wastewater treatment plant) of Guillarei, Tui, Galicia. This WTP remediated the municipal effluents by primary treatment (after filtration) and subsequent secondary treatment (after biological remediation). The characteristics of those effluents are provided in the supplementary material (Table S1). All experiences were performed in duplicate, and the deviation was found to be smaller than 4.3%. Consequently, the graphs show the average values.

### *4.4. Characterization*

#### 4.4.1. X-ray Diffraction (XRD)

Room-temperature XRD was carried out on a Rigaku diffractometer with an X PERT PRO MRD (Pananalytical, MA, USA) using Cu-K$\alpha$ radiation ($\lambda$ = 1.54187 Å). Each pattern was recorded in the 2$\theta$ range from 20° to 80° with a step of 0.03° and a total collection time of 2 h. The analysis of XRD patterns was carried out with Higscore software (Pananalytical, MA, USA).

#### 4.4.2. Raman

Raman spectra were collected using the Jobin Yvon HR800UV spectrometer (Horiba, Kyoto, Japan) equipped with Ar laser.

#### 4.4.3. SEM, EDS, and ICP

SEM and EDS analyses were completed using the microscope JSM-6700 F (JEOL, Tokyo, Japan) (CACTI). Inductively coupled plasma (ICP) coupled to optical emission spectrometry (ICP-OES Optima 4300, PekinElmer, MA, USA) (CACTI) was used for measuring leaching after the experiments and the initial photocatalyst composition. For that, acid digestion of 0.25 mg of the catalyst was carried out by adding 5 mL $HNO_3$ 7 M at 120 °C for 2 h in a 100 mL autoclave.

#### 4.4.4. UV-Vis

UV-Vis spectra of the samples for band gap calculation (Tauc plot [2]) were measured in a 1% EtOH solution on the spectrophotometer (V-2550, Shimadzu, Kyoto, Japan). This equipment was also used for MB removal monitorization with time.

#### 4.4.5. Electrochemical Measurements

Electrochemical Impedance Spectroscopy (EIS) and Electrochemically Active Surface Area (ECSA) were measured using the Autolab PGSTAT302N of Metrohm (Herisau, Switzerland). A three-electrode system was used, with Pt as the counter electrode, the calomel electrode as the reference, and Ni-foam (1 $cm^2$) as the working electrode where the catalysts were impregnated. A total of 3 mg of the catalyst was dissolved in 630 µL of a mixture Nafion:EtOH (1:20). The experiences were performed in a 0.5 M $Na_2SO_4$ solution. EIS was measured on a frequency range of $10^5$–0.1 Hz with a sinusoidal perturbation of 10 mV. ECSA was measured in a range of 0.1 V at scan rates between 10 and 200 mV $s^{-1}$. Then, a linear trend was attained by plotting scan rate vs. the difference in current density between anodic and cathodic sweeps divided by two. The slope provided after linear fitting of this graph provided geometric double-layer capacitance (CDL). ECSA was calculated following Equation (3), where Cs is the specific capacitance and has a value of 40 µF $cm^{-2}$ for experiences on a 0.5 M $H_2SO_4$ media [45].

$$ECSA = CDL/Cs \quad (3)$$

## 5. Conclusions

The F-$TiO_2$ catalyst was easily synthesized in a one-step synthesis. This catalyst was characterized by several means (XRD, FTIR, EDS, band gap, EIS, and ECSA calculations) which anticipated the good performance (F-$TiO_2$ showed a high electron mobility, a small band gap, and an elevated surface area). Indeed, the results demonstrated that the photocatalytic activity was better than the previously reported data, even better than the commercial well performant $TiO_2$ from Degussa. The wide-open reactor was selected based on a preliminary test which highlighted the importance of reducing the solution depth and increasing the radiation surface. The effect of pollutant and photocatalyst concentration, the alternative of working in a long-pulse radiation procedure, and the effect of the working matrix was evaluated. The reactor set-up and the synthesized catalyst made possible the efficient treatment of methylene blue and bisphenol A even when being in real wastewater matrixes. $H_2O_2$ addition is presented as an alternative to improve the degradation and reusability process. Thus, given that photocatalysis is a clean and sustainable technology, the fact the photocatalyst is reusable and the process can be used for real wastewater treatment, this process could be studied at higher scale in order to open a path for real applications.

**Supplementary Materials:** The following supporting information can be downloaded at: https://www.mdpi.com/article/10.3390/catal12101190/s1, Figure S1: MB degradation (20 mg/L) with 800 mg/L of TiO2 under UV radiation on the open-wide reactor (black circles) or the narrow-open reactor (red triangles). The lines represent the pseudo-first order kinetic adjustment; Figure S2: MB degradation under UV radiation depending on the selected ratio Ti:F between 1:0.5 (triangles), 1:1 (circles) and 1:2 (squares) (A) and pseudo-first order kinetic constants (B); Figure S3: MB degradation under UV radiation depending on the catalyst concentration. 200 mg/L (circles), 400 mg/L (triangles), 800 mg/L (squares), 1600 mg/L (rhombus) and 3200 mg/L (crosses) where the lines are the pseudo-first kinetic adjustment and B) depicts the pseudo-first order kinetic constants; Figure S4: $TiO_2$ and F-$TiO_2$ XRD with their peaks assignment; Figure S5: SEM image of F-$TiO_2$ photocatalyst (A) with EDS analysis (B); Figure S6: UV-Vis spectra of $TiO_2$ (A) and F-$TiO_2$ (B) photo-catalyst with band gap calculation with Tau equation (embed graphs); Figure S7: CDL measurement of $TiO_2$ (A) and F-$TiO_2$ (B) by measuring CVs at different scan rates and plotting the j difference vs the scan rate (embedded figures); Figure S8. Proposed scaled-up reactor; Table S1: Real wastewaters used as working matrix for MC degradation; Table S2: Pseudo-first order kinetic constants for the MB and BPA degradation under UV radiation with 800 mg/L of F-$TiO_2$.

**Author Contributions:** Conceptualization, A.M.D.; Methodology, A.M.D.; Software, A.M.D. and I.N.; Validation, A.M.D.; Formal Analysis, A.M.D.; Investigation, A.M.D. and I.N.; Resources, M.P., M.Á.S. and Y.V.K.; Data Curation, A.M.D. and I.N.; Writing—Original Draft Preparation, A.M.D.; Writing—Review and Editing, M.P., M.Á.S. and Y.V.K.; Visualization, A.M.D.; Supervision, M.P., M.Á.S. and Y.V.K.; Project Administration, M.P., M.Á.S. and Y.V.K.; Funding Acquisition, A.M.D., M.P., M.Á.S. and Y.V.K. All authors have read and agreed to the published version of the manuscript.

**Funding:** This research was funded by Xunta de Galicia grant numbers ED481B 2019/091 and ED431C 2021-43. Additionally, the research has been provided with the financial support under the BiodivRestore ERA-Net COFUND programme, Project PCI2022-132941 funded by MCIN/AEI/10.13039/501100011033 and European Union Next Generation EU/PRTR and PID2020-113667GB-I00 funded by MCIN/AEI/10.13039/501100011033.

**Data Availability Statement:** Data is contained within the article and supplementary materials.

**Conflicts of Interest:** The authors declare no conflict of interest.

## References

1. Kurniawan, T.A.; Mengting, Z.; Fu, D.; Yeap, S.K.; Othman, M.H.D.; Avtar, R.; Ouyang, T. Functionalizing TiO2 with graphene oxide for enhancing photocatalytic degradation of methylene blue (MB) in contaminated wastewater. *J. Environ. Manag.* **2020**, *270*, 110871–110879.
2. Zhang, X.; Chen, W.; Bahmanrokh, G.; Kumar, V.; Ho, N.; Koshy, P.; Sorrell, C.C. Synthesis of V- and Mo-doped/codoped $TiO_2$ powders for photocatalytic degradation of methylene blue. *Nano-Struct. Nano-Objects* **2020**, *24*, 100557–100568.

3. D'Souza, L.P.; Prakash, R.M.; Balakrishna, R.G. Chapter 3 Anion-Modified Photocatalysts. In *Photocatalytic Systems by Design*; Sakar, M., Balakrishna, R.G., Do, T., Eds.; Elsevier: Amsterdam, The Netherlands, 2021, p. 55–83.
4. Jafari, A.J.; Kalantary, R.R.; Esrafili, A.; Moslemzadeh, M. Photo-catalytic degradation of bisphenol-a from aqueous solutions using GF/Fe-$TiO_2$-CQD hybrid composite. *J. Environ. Health Sci. Eng.* **2021**, *19*, 837–849.
5. Humayun, M.; Raziq, F.; Khan, A.; Luo, W. Modification strategies of $TiO_2$ for potential applications in photocatalysis: A critical review. *Green Chem. Lett. Rev.* **2018**, *11*, 86–102.
6. Chakinala, N.; Gogate, R.R.; Chakinala, G. Highly efficient bi-metallic bismuth-silver doped $TiO_2$ photocatalyst for dye degradation. *Korean J. Chem. Eng.* **2021**, *38*, 2468–2478.
7. Zheng, X.; Han, H.; Ye, X.; Meng, S.; Zhao, S.; Wang, X.;Chen, S. Fabrication of Z-scheme $WO_3$/$KNbO_3$ photocatalyst with enhanced separation of charge carriers. *Chem. Res. Chin. Univ.* **2020**, *36*, 901–907.
8. Hunge, Y.M.; Yadav, A.A.; Khan, S.; Takagi, K.; Suzuki, N.; Teshima, K.; Terashima, C.; Fujishima, A. Photocatalytic degradation of bisphenol A using titanium dioxide@ nanodiamond composites under UV light illumination. *J. Colloid. Interface Sci.* **2021**, *582*, 1058–1066.
9. Acosta-Esparza, M.A.; Rivera, L.P.; Pérez-Centeno, A.; Zamudio-Ojeda, A.; González, D.R.; Chávez-Chávez, A.; Santana-Aranda, M.A.; Santos-Cruz, J.; Quiñones-Galván, J. UV and Visible light photodegradation of methylene blue with graphene decorated titanium dioxide. *Mater. Res. Express.* **2020**, 7, 35504–35512.
10. Bibi, S.; Ahmad, A.; Anjum, M.A.R.; Haleem, A.; Siddiq, M.; Shah, S.S.; Kahtani, A.A. Photocatalytic degradation of malachite green and methylene blue over reduced graphene oxide (rGO) based metal oxides (rGO-$Fe_3O_4$/$TiO_2$) nanocomposite under UV-visible light irradiation. *J. Environ. Chem. Eng.* **2021**, *9*, 105580–105591.
11. Badvi, K.; Javanbakht, V. Enhanced photocatalytic degradation of dye contaminants with $TiO_2$ immobilized on ZSM-5 zeolite modified with nickel nanoparticles. *J. Clean Prod.* **2021**, *280*, 124518–124531.
12. Niu, L.; Zhao, X.; Tang, Z.; Lv, H.; Wu, F.; Wang, X.; Zhao, T.; Wang, J.; Wu, A.; Giesy, J. Difference in performance and mechanism for methylene blue when $TiO_2$ nanoparticles are converted to nanotubes. *J. Clean Prod.* **2021**, *297*, 126498–126509.
13. Shayegan, Z.; Lee, C.; Haghighat, F. Effect of surface fluorination of P25-$TiO_2$ coated on nickel substrate for photocatalytic oxidation of methyl ethyl ketone in indoor environments. *J. Environ. Chem. Eng.* **2019**, *7*, 103390–103401.
14. Gao, Q.; Si, F.; Zhang, S.; Fang, Y.; Chen, X.; Yang, S. Hydrogenated F-doped $TiO_2$ for photocatalytic hydrogen evolution and pollutant degradation. *Int. J. Hydrog. Energy* **2019**, *44*, 8011–8019.
15. Rani, M.; Keshu Shanker, U. Efficient degradation of organic pollutants by novel titanium dioxide coupled bismuth oxide nanocomposite: Green synthesis, kinetics and photoactivity. *J. Environ. Manag.* **2021**, *300*, 113777–113791.
16. Shiraishi, F.; Ueno, M.; Chand, R.; Shibata, Y.; Luitel, H.N. Effect of silanization of titanium dioxide on photocatalytic decomposition of 2,4-dinitropheonol under irradiation with artificial UV light and sunlight. *J. Chem. Technol. Biotechnol.* **2014**, *89*, 81–87.
17. Habib, I.Y.; Burhan, J.; Jaladi, F.; Lim, C.M.; Usman, A.; Kumara, N.T.R.N.; Tsang, S.C.E.; Mahadi, A.H. Effect of Cr doping in CeO2 nanostructures on photocatalysis and $H_2O_2$ assisted methylene blue dye degradation. *Catalysis Today* **202**0, *375*, 506–513.
18. Diao, W.; Xu, J.; Rao, X.; Zhang, Y. Facile Synthesis of Fluorine Doped Rutile TiO2 Nanorod Arrays for Photocatalytic Removal of Formaldehyde. *Catal. Lett.* **2022**, *152*, 1029–1039.
19. Ahmad, N.; Sultana, S.; Sabir, S.; Khan, M.Z. Exploring the visible light driven photocatalysis by reduced graphene oxide supported Ppy/CdS nanocomposites for the degradation of organic pollutants. *J. Photochem. Photobiol. A* **2020**, *386*, 112129–112142.
20. Ângelo, J.; Magalhães, P.; Andrade, L.; Mendes, A. Characterization of $TiO_2$-based semiconductors for photocatalysis by electrochemical impedance spectroscopy. *Appl. Surf. Sci.* **2016**, *387*, 183–189.
21. Díez, A.M.; Valencia, H.E.; Meledina, M.; Mayer, J.; Kolen'ko, Y.V. Photocatalytic-fenton process under simulated solar radiation promoted by a suitable catalyst selection. *Catalysts* **2021**, *11*, 885–897.
22. Lian, X.; Chen, S.; He, F.; Dong, S.; Liu, E.; Li, H.;Xu, K.. Photocatalytic degradation of ammonium dinitramide over novel S-scheme g-C3N4/BiOBr heterostructure nanosheets. *Sep. Purif. Technol.* **2022**, *286*, 120449–120459.
23. Garg, R.; Gupta, R.; Bansal, A. Degradation mechanism, reaction pathways and kinetics for the mineralization of Bisphenol A using hybrid ZnO/graphene oxide nano-catalysts. *Korean J. Chem. Eng.* **2021**, *38*, 485–497.
24. Arias, M.C.; Aguilar, C.; Piza, M.; Zarazua, E.; Anguebes, F.; Cordova, V. Removal of the Methylene Blue Dye (MB) with Catalysts of Au-$TiO_2$: Kinetic and Degradation Pathway. *Mod. Res. Catal.* **2021**, *10*, 1–14.
25. Brahmi, C.; Benltifa, M.; Ghali, M.; Dumur, F.; Simonnet-Jégat, C.; Monnier, V.; Morlet-Savary, F.; Bousselmi, L.; Lalevée, J. Polyoxometalates/polymer composites for the photodegradation of bisphenol-A. *J. Appl. Polym. Sci.* **2021**, *138*, 50864–50876.
26. Pupo Nogueira, R.F.; Trovó, A.G.; Modé, D.F. Solar photodegradation of dichloroacetic acid and 2,4-dichlorophenol using an enhanced photo-Fenton process. *Chemosphere* **2002**, *48*, 385–391.
27. Bangun, J.; Adesina, A.A. The photodegradation kinetics of aqueous sodium oxalate solution using $TiO_2$ catalyst. *Appl. Catal. A Gen.* **1998**, *175*, 221–235.
28. Sun, X.; Xu, K.; Chatzitakis, A.; Norby, T. Photocatalytic generation of gas phase reactive oxygen species from adsorbed water: Remote action and electrochemical detection. *J. Environ. Chem. Eng.* **2021**, *9*, 104809–104818.
29. Pascariu, P.; Cojocaru, C.; Samoila, P.; Airinei, A.; Olaru, N.; Rusu, D.; Rosca, I.; Suchea, M. Photocatalytic and antimicrobial activity of electrospun ZnO:Ag nanostructures. *J. Alloy. Compd.* **2020**, *834*, 155144–155155.
30. Arunagiri, C. *Enhanced Visible Light Photocatalytic Degradation of Fe-Doped ZnO Nanoparticles For Organic Dyes*; Research Square, Newcastle, Unit Kingdom, 2021.

31. Peng, H.; Xu, L.; Zhang, W.; Liu, F.; Lu, X.; Lu, W.; Danish, M.; Lin, K. Different kinds of persulfate activation with base for the oxidation and mechanism of BDE209 in a spiked soil system. *Sci. Total Environ.* **2017**, *574*, 307–313.
32. Subalakshmi, K.; Senthilselvan, J. Effect of fluorine-doped $TiO_2$ photoanode on electron transport, recombination dynamics and improved DSSC efficiency. *Sol. Energy* **2018**, *171*, 914–928.
33. Noh, K.; Oh, H.; Bo-Ra, K.; Jung, S.; Kang, W.; Sun-Jae, K. Photoelectrochemical Properties of $Fe_2O_3$ Supported on TiO2-Based Thin Films Converted from Self-Assembled Hydrogen Titanate Nanotube Powders. *J. Nanomater.* **2012**, 2012, 1–6.
34. Mahanta, U.; Khandelwal, M.; Deshpande, A.S. $TiO_2$@$SiO_2$ nanoparticles for methylene blue removal and photocatalytic degradation under natural sunlight and low-power UV light. *Appl. Surf. Sci.* **2022**, *576*, 151745–151756.
35. Pant, B.; Ojha, G.P.; Kuk, Y.; Kwon, O.H.; Park, Y.W.; Park, M. Synthesis and Characterization of ZnO-$TiO_2$/Carbon Fiber Composite with Enhanced Photocatalytic Properties. *Nanomaterials* **2020**, *10*, 1960–1971.
36. Mahanthappa, M.; Kottam, N.; Yellappa, S. Enhanced photocatalytic degradation of methylene blue dye using CuSCdS nanocomposite under visible light irradiation. *Appl. Surf. Sci.* **2019**, *475*, 828–838.
37. Liu, J.; Shi, H.; Sans, C.; Sun, L.; Yuan, X.; Pan, F.; Xia, D . Insights into the photocatalytic ozonation over $Ag_2O$-ZnO@g-C3N4 composite: Cooperative structure, degradation performance, and synergistic mechanisms. *J. Environ. Chem. Eng.* **2022**, *10*, 107285–107298.
38. Sultana, S.; Ahmad, N.; Ahmad, E.; Sabir, S.; Khan, M.Z. Electrochemical synthesis of novel aluminium oxyhydroxide-decorated $MnO_2$/chitosan nanocomposite with efficient photocatalytic and antibacterial activity. *Nanotechnol. Environ. Eng.* **2020**, *5*, 20.
39. Peng, X.; Zhang, Y.; Liu, Y. Fabrication of a novel high photocatalytic Ag/$Ag_3PO_4$/P25 ($TiO_2$) heterojunction catalyst for reducing electron-hole pair recombination and improving photo-corrosion. *Mater. Res. Express.* **2019**, *6*, 65515–65525.
40. Arifin, M.N.; Rezaul Karim, K.M.; Abdullah, H.; Khan, M.R. Synthesis of titania doped copper ferrite photocatalyst and its photoactivity towards methylene blue degradation under visible light irradiation. *Bull. Chem. React. Eng. Catal.* **2019**, *14*, 219–227.
41. Chen, H.; Luo, S.; Lei, X.; Liu, H.; Liu, Y.; Xu, X.; Jiang, Z.; Li, X. Synthesis and photocatalytic performance of nano-$CeO_2$ by a PVP-assisted microwave interface method for organic dye degradation. *Ionics* **2020**, *26*, 5829–5839.
42. Murcia, J.J.; Cely, Á.C.; Rojas, H.A.; Hidalgo, M.C.; Navío, J.A. Fluorinated and platinized titania as effective materials in the photocatalytic treatment of dyestuffs and stained wastewater coming from handicrafts factories. *Catalysts* **2019**, *9*, 179–199.
43. Titchou, F.E.; Zazou, H.; Afanga, H.; El Gaayda, J.; Ait Akbour, R.; Nidheesh, P.V.; Hamdani, M. Removal of organic pollutants from wastewater by advanced oxidation processes and its combination with membrane processes. *Chem. Eng. Process. Process Intensif.* **2021**, *169*, 108631–108653.
44. Pham, D.C.; Cao, T.M.D.; Nguyen, M.C.; Nguyen, T.D.; Nguyen, V.H.; Bui, V.H.; Nguyen, T.T.T. Integrating Photocatalysis and Microfiltration for Methylene Blue Degradation: Kinetics and Cost Estimation. *Chem. Eng. Technol.* **2022**, *45*, 1748–1758.
45. Coleman, N.; Lovander, M.D.; Leddy, J.; Gillan, E.G. Phosphorus-Rich Metal Phosphides: Direct and Tin Flux-Assisted Synthesis and Evaluation as Hydrogen Evolution Electrocatalysts. *Inorg. Chem.* **2019**, *58*, 5013–5024.